Optical Effects of Intraocular Gas Tamponade

Joseph E. Shepherd[1]

March 23, 2019

Abstract Optical effects associated with refraction created by intraocular gas tamponade following retina surgery are reported and analyzed. Observations of dramatic change in both near point and magnification are explained using ray tracing and simplified models of the eye as an optical system. The gas bubble shapes are computed using the Young-Laplace law and compared to previous clinical measurements and analyses. The effect of bubble shape on refraction is determined by including the curvature of the gas-liquid interface on the optical axis of a downward facing eye. A possible clinical application is the estimation of gas volume from near point measurements.

1 Introduction

Following the vitrectomy, photocoagulation treatment of lattice thinning and removal of an epiretinal membrane on my right eye, the intraocular volume was partially filled with gas (SF_6/air mixture). For several days following the surgery, my perception in that eye was quite limited and I noticed only vague shapes and colors. Quite by accident one day, I brought the screen of my cell phone close to my face while I was looking directly downward as in Figure 1 and was startled to see an enlarged image of the icons in my right eye. After some experimentation with various objects (like my keyboard shown in the simulated image of Fig. 1) at different distances from my eye, I realized that the gas layer between the retina and fluid that partially filling the intraocular cavity was altering the optics of the eye to produce a magnifying glass effect. As the gas "bubble" was absorbed in following days, I noticed that the distance at which I could bring objects to focus was becoming progressively further from my eye. At the same time, I could see more of the meniscus between the vitreous humor and the retina at the periphery of my vision when looking downward.

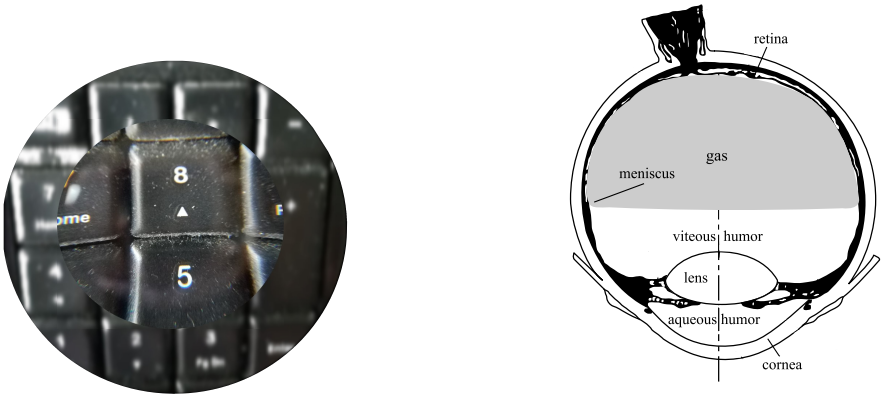

Figure 1: Left: Simulation of visual effect I observed looking downward through the gas bubble in my eye. Right: Geometry of a large gas bubble within the eye looking directly downward with a vertical optical axis.

2 Optical Analysis

Intrigued by this effect I set out to find an explanation using the science of optics. To do this, I needed a model of the eye as an optical system and a method of optical analysis that could account for the effects of the gas layer. The century-old schematic model of the eye by Gullstrand (see Appendix II in von Helmholtz, 1924) is appropriate for our purposes with modern values of the parameters (Gross et al., 2015). Geometrical optics is the oldest and simplest method of optical analysis and is adequate for our investigation of the properties of focal distance and magnification.

[1]Graduate Aerospace Laboratories, California Institute of Technology, Pasadena, CA 91125 USA. jeshep@caltech.edu

Geometrical optics is based on tracing representative rays of light through the optical components to determine the location and size of images, applying Snell's law to compute refraction; the details of the ray tracing and eye model are given at the end of this note. The first model of the gas layer I investigated assumed that the layer was flat near the optical axis. This turns out to be a reasonable approximation for gas volumes greater than 1.5 to 2 cm^3 (layers greater than 10 mm thick) but not for smaller gas volumes.

Example rays and the effect of gas are shown in the diagrams of Figure 2 for both the relaxed eye model (left column) and the accommodation variant (right column). Only the upper half of the eye is shown because these schematic models are symmetric about the optical axis of the eye. To make the calculations simple, we will consider the object and image to be on the optical axis although in the real eye these are slightly off-axis due to the displacement of the macula, where the image is usually centered. The top row of diagrams shows results for the normal (no gas) eye with the source placed at the conjugate focus to the retina[2] of the eye to simulate the formation of an image on the retina as indicated by the convergence of the rays to the point where the optical axis intersects the retina. The middle row of diagrams shows the effect of leaving the object at the same location and adding a 10 mm gas layer.[3] The convergence of the rays to a point within the gas layer indicates that the image is focused several mm ahead of the retina, as in the myopic eye, and the image on the retina will be out of focus, which explains the blurry images experienced when looking through the gas bubble at objects far away from the eye. The convergence of the rays before reaching the retina is a consequence of Snell's law: rays passing from the higher refractive index (n = 1.336) vitreous humor into the much lower refractive index ($n \approx 1$) gas are bent away from the normal to the interface, toward the optical axis.

The bottom row illustrates what happens when the object is brought closer to eye and located at the conjugate focus.[4] The rays now converge to a point on the retina and will form a focused image. This is the effect that I observed when bringing my cell phone screen close to my right eye. The near point (closest distance at which a focused image can be formed) can be approximated as the location of conjugate focus. As shown in Figure 3, the near point decreases with increasing thickness of the gas layer, reaching a minimum value of 58 to 82 mm (depending on the eye model) from the vertex (z = 0) of the cornea when the intraocular space is completely filled with gas.

When holding the head in a tilted position rather than looking straight downward, objects located close to the eye can still be imaged but appeared displaced in position compared to the location observed by the other eye or region of the retina not covered by gas This effect is due to the refraction of light passing obliquely through the gas-vitreous humor interface as shown in Figure 4. Light is not only refracted in passing through the interface but also reflected. If there are bright lights within the field of view and I hold my head up so that the gas moves to the top of my eye, these reflections will be visible as streaks of light when the gas bubble is sufficiently small that the retina is covered by vitreous fluid in the peripheral regions. When the angle of incidence[5] exceeds the critical angle of 48.4°, the incident light is completely reflected and the region within the meniscus will appear as a dark semi-ellipsoidal region at the bottom of my field of vision. The intensity of light observed through the meniscus region will continuously decrease as I change my gaze by rotating my head from looking directly downward until my gaze is elevated upward at the critical angle. This corresponds to a gaze angle of approximately 45° downward from the horizontal. The meniscus is perceived at the bottom of the field of vision and the streaks at the top due to inversion carried out by the vision processing of the brain.

What about the magnification effect? The refraction of the rays at the gas-vitreous humor interface also changes the size of the image on the retina compared to the size without the gas layer. This is a consequence of moving the near point closer the eye, the same effect occurs when using a magnifying glass on a normal eye. For example, a typical 5-power magnifying glass (a lens with a focal length of 50 mm) held 25 mm from the cornea of our accommodation model eye will image an object held at distance of 41 mm from the lens and the image on the retina will be 5.5 times larger than the image of the same object held at the near point (250 mm from the cornea) without magnification. The magnifying effect of gas layer with a flat interface at the optical axis is found to increase linearly with increasing layer thickness for the accommodation model eyes. The lateral magnification with a 10 mm gas layer is 4 for the 250 mm near point model eye and 12 for the 1000 mm near point model eye.

[2]The conjugate focus is measured relative to the vertex of the cornea and located at infinity for the relaxed eye model and either 250 or 1000 mm for the accommodation variants I examined.

[3]The situation shown corresponds to looking straight down as in the eye diagram above so that so that the gas-vitreous humor interface is horizontal and perpendicular to the optical axis.

[4]With the 10 mm gas layer, the location of the conjugate focus is 126 mm for the relaxed eye model, and 88 mm for the accommodation variant with 250 mm near point and 93 mm for the 1000 mm near point eye model.

[5]The convention in optics is that incidence angle is measured relative to the direction perpendicular to surface on the side the light is incident from, in this case on the vitreous humor side of the interface with gas.

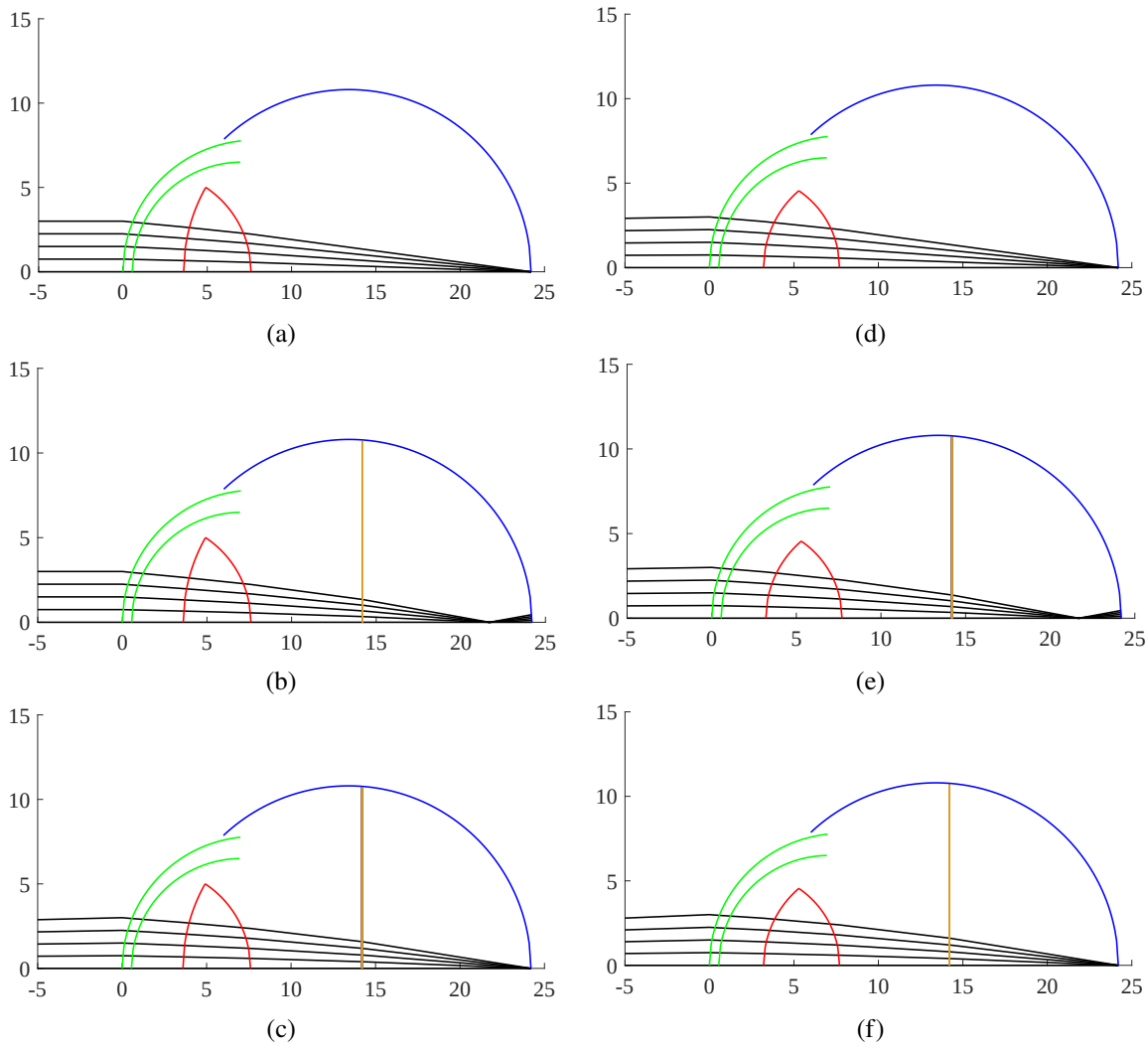

Figure 2: Light rays illustrating the effect of a gas layer (with a flat interface at the optical axis) on the focusing ability of the eye. Left column (a, b c) - relaxed eye model of Gullstrand-Le Grand. Right column (d, e, f) - accommodation model variant of Gullstrand-Le Grand model. Top row - normal eye with object at the conjugate focus of the retina. Middle row - same as top row with addition of a 10 mm thick layer of gas. Bottom row - same as middle row except the object is moved to the conjugate focus of retina.

3 Bubble Shape Effects

As the gas bubble shrinks, the gas-vitreous interface becomes increasingly curved (see Figure 5) due to surface tension,[6] eventually forming a nearly spherical bubble for sufficiently small amounts of gas. This creates two additional optical effects. First, the refraction of light through the curved interface at the optical axis reduces the intensity of light reaching the retina, creating a continuous decrease in intensity from the center to the edge of the bubble, which appears completely dark with sharp transition to the surrounding bright field. Second, the curved interface acts as lens with a negative focal length, which causes the near point for images formed within the bubble region to recede as the bubble shrinks. Assuming a head-down position with a vertical optical axis, we can analyze this optical effect by determining the curvature (Figure 5) of the interface near the optical axis from the the shape of the bubble. The shape of the bubble is determined by the competing forces of buoyancy and interfacial forces and is computed using the Young-Laplace

[6]The curvature of the interface and the meniscus effect due to the contact angle and surface tension can be clearly observed in CT (see Fig. 6 and 7 of Hilton and Grizzard (1986)) and MRI scans (see Fig. 11 and 12 of Ito (2016)).

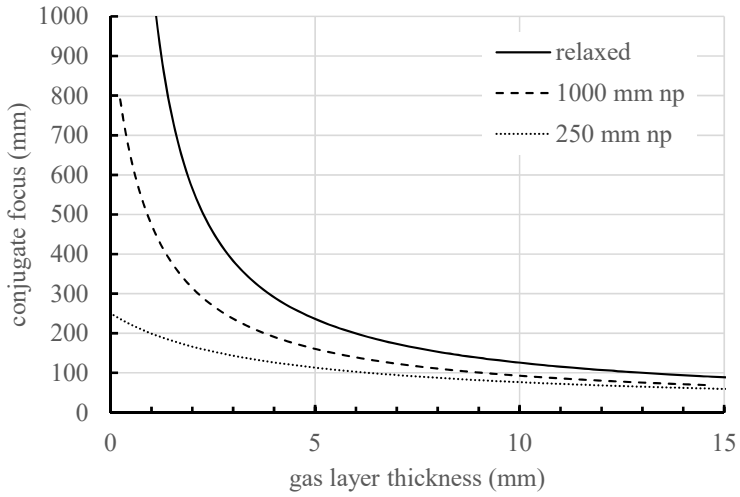

Figure 3: Conjugate focus location as a function of gas layer thickness for both the relaxed eye model and two accommodation models. Results obtained with a flat interface at the optical axis.

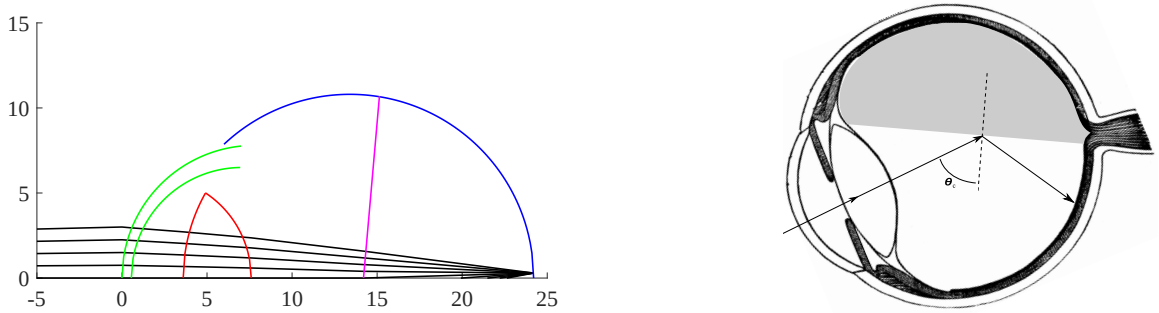

Figure 4: Optical effects at the vitreous humour-gas interface. Left: refraction. Right: total internal reflection (artwork from `http://etc.usf.edu/clipart/`).

equation and methods of analysis pioneered by Adams (Bashforth and Adams, 1883).

The optical effect of the curvature of the vitreous humor-gas interface can be treated in the ray tracing computation by setting the interface radius of curvature at the optical axis equal to that computed by the Young-Laplace model. The smaller the gas volume and interface layer thickness, the greater the curvature at the optical axis. The result is that the magnification is reduced and the near point increased from the flat interface values. The magnification and near point have the same trends with decreasing gas layer height for both flat and curved interfaces until the layer becomes less than 2.1 mm thick (gas volume less than 0.05 cm^3).

For the two accommodation eye models with the curved interface effect included, the conjugate focus location does not increase monotonically with decreasing gas layer thickness but achieves a maximum value that is larger than the gas-free near point value for a layer thickness of about 2 mm as shown in Figure 6. This effect is very pronounced for the 1000 mm (1 Diopter) near point eye model so that older patients (> 60 yr old) or those with a fixed focal length due to an IOL will experience a very pronounced change in near point within the visual field subtended by the gas bubble as the gas bubble shrinks.[7]

Another effect of the curvature is on the relationship between gas volume and retina coverage. From a clinical viewpoint, sufficient gas volume needs to be injected to cover the portion of retina being treated. Based on observations of gas injection into a plastic spherical eye model, Parver and Lincoff (1978) proposed that the relationship could be based on modeling the interface as flat. While this is appropriate for large volumes, as first noted by Hilton and Grizzard (1986) in their clinical studies using computerized tomography (CT) to determine angular coverage and gas volume,

[7]In the final stages of the gas bubble dissolution, I estimated that the near point was at least 1 m from my eye, which has an IOL with a normal fixed near point of 1 Diopter.

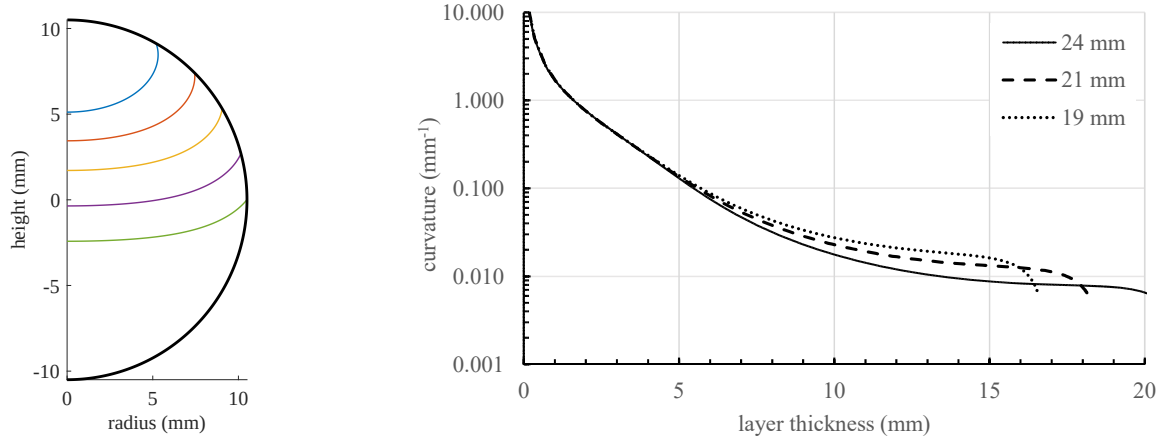

Figure 5: Vitreous humour-gas interface in head down position. Left: representative shapes corresponding to the cases in Table 1 for 21 mm diameter eye. Right: reciprocal of the radius of curvature at optical axis as a function of gas layer thickness as measured along the optical axis from the bottom of the bubble to the retina. Results for three eye diameters with common interface parameters θ_c = 39° (contact angle) and γ = 0.070 N/m (surface tension).

the Parver and Lincoff model significantly overestimates coverage for gas bubbles less than 2 ml. The Young-Laplace solution also predicts significantly smaller coverage areas than the Parver and Lincoff and is consistent with the CT results if the non-spherical shape of the eye is taken into account (Figure 7). Clinical practice (Hilton et al., 1996) apparently relies on gas volumes based on the CT studies of Hilton and Grizzard with a volume of 0.3 cm^3 for 60° coverage and 1.2 cm^3 for 90° coverage of the retina. Hilton et al. also note that a highly myopic eye with a large globe will require a larger amount of gas to cover the same surface area. The Young-Laplace model with the nominal values of surface tension and contact angle are consistent with the clinical studies if the variation in eye shape between individuals and the nonspherical shape of the eye is taken into account (see Table 1 and Figure 7).

The volume of gas needed to cover a given angle of the retina is for practical purposes, directly proportion to the volume of the eye, so that the volumes required for the 24 mm diameter eye are $(24/19)^3$ or 2 $\times$ larger than for the 19 mm diameter eye. The Young-Laplace model for a 21 mm diameter eye, assumed to be the nominal emmetropic dimension, overpredicts the coverage angle for a given volume in comparison with the clinical data of Hilton and Grizzard. Comparisons of the entire CT data set of Hilton and Grizzard (Figure 7) with the Young-Laplace model using a range of effective eye diameters indicates that an effective diameter of 22 mm appear appropriate for the larger coverage angles (182, 187, and 290°) but a much larger effective diameter (26 mm) is more consistent with the data for a coverage angle less than 90°. For coverage angles less than 120°, the Parver and Lincoff flat interface model underpredicts the required gas volume by a minimum of a factor of two and as much as a factor of 5 at 60°.

Table 1: Gas volumes V and associated bubble heights h required to produce a specified angular coverage of the retina for three eye diameters using a spherical model for the intraocular cavity.

	eye diameter					
	24 mm		21 mm		19 mm	
Coverage (deg)	V (cm^3)	h (mm)	V (cm^3)	h (mm)	V (cm^3)	h (mm)
60	0.45	5.8	0.32	5.4	0.25	5.1
90	1.08	7.6	0.75	7.0	0.59	6.7
120	2.00	9.7	1.40	8.8	1.07	8.3
150	3.15	12.0	2.16	10.8	1.63	10.0
180	4.36	14.4	2.97	12.9	2.22	11.9

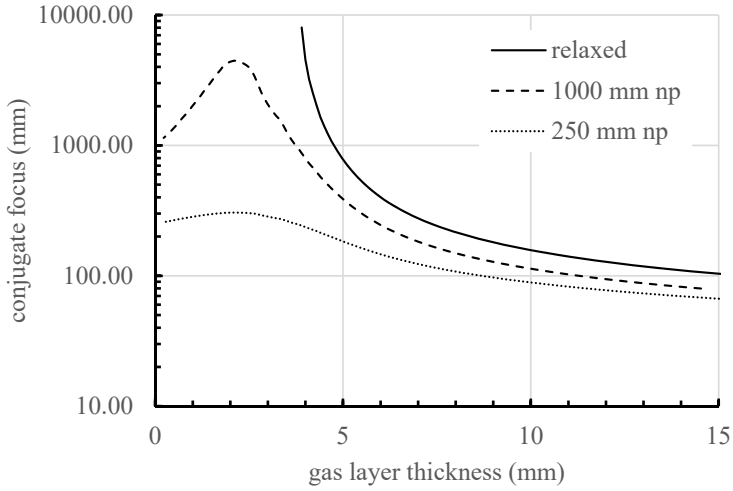

Figure 6: Conjugate focus location as a function of gas layer thickness for three eye models using the curved interface computed with the Young-Laplace model.

4 A Potential Clinical Application

If the near point of the eye without a gas layer is known or can be approximated, then the gas volume can be estimated from measurements of the conjugate focus with the gas-filled eye. An example of the gas volume-conjugate focus relationship is shown in the upper graph of Figure 8 for two eye accommodation models using the curved interface results for a 21 mm eye model. These predictions are consistent with my own experience. Using the bridge of my nose as a surrogate for the location of my corneal vertex, I estimated a value of about 90 to 100 mm for the near point 8 days after my surgery; this increased to about 200 to 220 mm at 14 days when the bubble had shrunk to about 15% of the original volume. Just before the bubble disappeared from my eye, I estimated that the near point had approached 1 m.

As discussed above, there is also a significant magnification effect which potentially could be used to estimate gas bubble volume with the aid of the lower graph of Figure 8. However to utilize the magnification effect in conjunction with the perceived extent of the bubble, rays with large angles from the optical axis will have to be considered. Such analyses would need to use a more sophisticated description of the eye optical elements as having aspheric surfaces in order to treat rays that are far from the optical axis; eye models with this sophistication are available and are reasonably straightforward to use in modern optical analysis software (Greivenkamp et al., 1995).

Acknowledgement

I am grateful to my opthamologists who treated my cataract and retina conditions: Sunil Bhandarkar, M.D. of Larchmont Eye Care and Daniel D. Esmaili, M.D. of Retina Vitreous Associates Medical Group. Dr. Esmaili suggested the potential clinical application of the gas layer optical effect in estimating gas bubble volume.

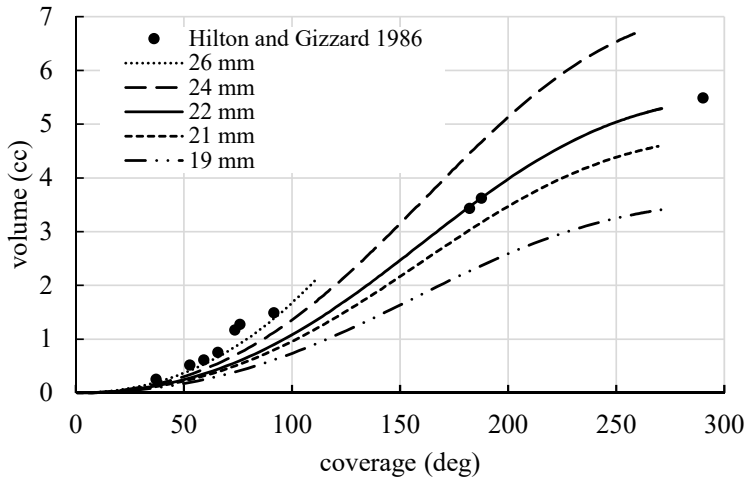

Figure 7: Comparison of the Hilton and Grizzard CT data with eye models of various mean diameters and using the Young-Laplace model to compute the bubble volume and coverage angle.

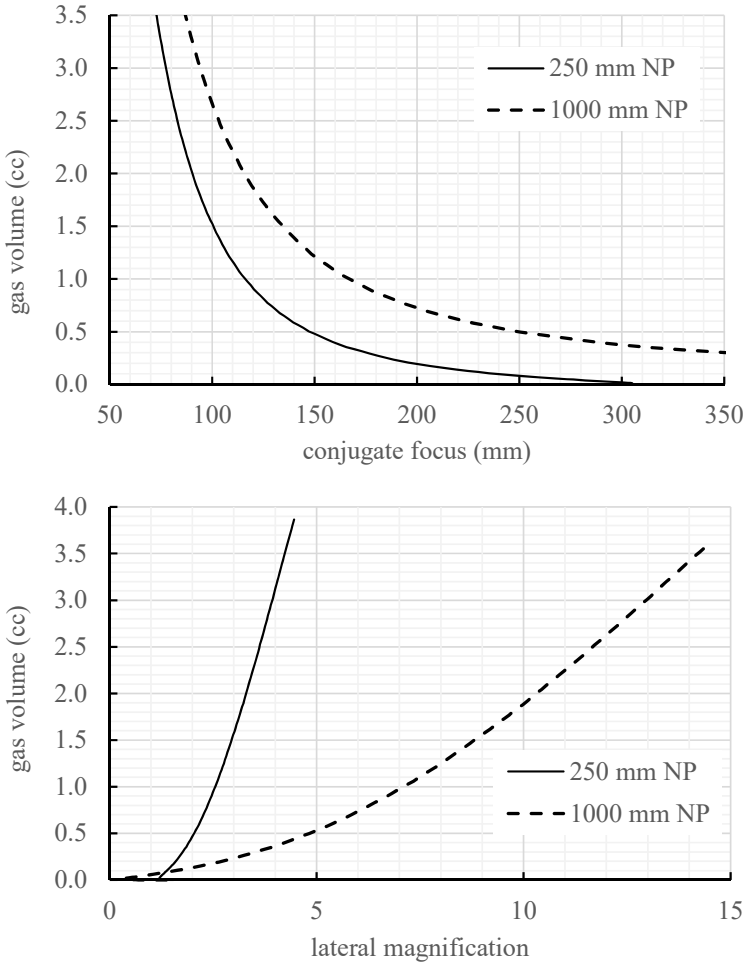

Figure 8: Relationship of gas volume to conjugate focus location and magnification predicted for two accommodated eye models with near points of 1000 and 250 mm (1 and 4 Diopter) and using the Young-Laplace model of interface curvature for a 21 mm diameter eye.

References

David A. Atchison. Optical models for human myopic eyes. *Vision Research*, 46(14):2236–2250, July 2006. doi: 10.1016/j.visres.2006.01.004.

F. Bashforth and J.C. Adams. *An Attempt to Test the Theories of Capillary Action by Comparing The Theoretical and Measured Forms of Drops of Fluid*. Cambridge University Press, 1883.

G.K. Batchelor. *An Introduction to Fluid Dynamics*. Cambridge University Press, 1967.

Eugene de Juan, Brooks McCuen, and James Tiedeman. Intraocular tamponade and surface tension. *Survey of Ophthalmology*, 30(1):47–51, July 1985. doi: 10.1016/0039-6257(85)90088-8.

Ian Eames, Romesh I. Angunawela, G. William Aylward, and Ali Azarbadegan. A Theoretical Model for Predicting Interfacial Relationships of Retinal Tamponades. *Investigative Ophthalmology & Visual Science*, 51(4):2243, April 2010. doi: 10.1167/iovs.09-4442.

I.M. Fawcett, R.L. Williams, and D Wong. Contact angles of substances used for internal tamponade in retinal detachment surgery. *Graefe's Arch Clin Exp Ophthalmol*, 232:438–444, 1994.

M T Flores-Arias, A Díaz del Rio, C Bao-Varela, M V Pérez, and C Gómez-Reino. Description of gradient-index human eye by a first-order optical system. *Journal of Optics A: Pure and Applied Optics*, 11(12):125301, December 2009. doi: 10.1088/1464-4258/11/12/125301.

G.R. Fowles. *Introduction to Modern Optics*. Holt, Reinhart and Winston, 2nd edition, 1975.

H.H. Goldstine. *A History of Numerical Analysis from the 16th through the 19th century*, volume 2 of *Studies in the History of Mathematics and Physical Sciences*. Springer Verlag, 1977.

John E. Greivenkamp, Jim Schwiegerling, Joseph M. Miller, and Mark D. Mellinger. Visual Acuity Modeling Using Optical Raytracing of Schematic Eyes. *American Journal of Ophthalmology*, 120(2):227–240, August 1995. doi: 10.1016/S0002-9394(14)72611-X.

Herbert Gross, Fritz Blechinger, and Bertram Achtner. Human Eye. In *Survey of Optical Instruments*, volume 4 of *Handbook of optical systems*. Wiley-VCH, Weinheim, 2015. doi: 10.1002/9783527699247.ch1.

D.J. Hayes. *Studies of Refrigerant Gases for Use in Cherenkov Detectors at Jefferson Lab*. B.S. Thesis, College of William and Mary in Virginia, Williamsburg, VA, May 2018.

George F Hilton and W.S. Grizzard. Pneumatic retinopexy: A two-step outpatient operation without conjunctival incision. *Ophthalmology*, 93:626–640, 1986. doi: 10.1016/S0161-6420(86)33696-0.

George F Hilton, Taraprasad Das, Ajit B Majji, and Subhadra Jalali. Pneumatic retinopexy: principles and practice. *Indian Journal of Opthamology*, 44(3):131–143, 1996.

Yusuke Ito. Imaging characteristics of the postoperative globe: Pictorial review, 2016. URL `http://epos.myesr.org/poster/ecr2016//C-1333`.

Rafael Navarro. The Optical Design of the Human Eye: a Critical Review. *Journal of Optometry*, 2(1):3–18, 2009. doi: 10.3921/joptom.2009.3.

Barrett O'Neill. *Elementary Differential Geometry*. Academic Press, 1966.

L.M. Parver and H Lincoff. Mechanics of intraocular gas. *Investigative Ophthalmology & Visual Science*, 17(1):77–79, January 1978.

H. von Helmholtz. *Helmholtz's Physiological Optics*, volume 1. The Optical Society of America, translation from the 3rd German edition, 1924.

Supplement: Analysis Methodologies

5 Ray Tracing

Ray tracing (Fowles, 1975, Ch. 10) is the process of simulating light by imagining the light emission from a point can be modeled as a bundle of rays or lines that move on straight paths and only bend (refract) at interfaces such as the surface between air and water.

For a simple optical system with components like lenses placed symmetrically on line (the z axis), a point on a ray can be described by the angle with the axis θ and the perpendicular distance ρ from the z-axis. For small angles θ, all the rays are sufficiently close to the axis that computations can be simplified by making the *paraxial* approximation that the locations of the surfaces of interfaces, although curved, can be approximated as planes perpendicular to the optical axis and the sine of the angle can be approximated by the angle itself.

The parameters of the ray can be specified by a column vector and the effect on the ray of passing through the optical system can be specified by a matrix $[M]$. The parameters at location z_2 are related to those at location z_1 by matrix multiplication.

$$\begin{bmatrix}\rho\\ \theta\end{bmatrix}_2 = \begin{bmatrix}M_{11} & M_{12}\\ M_{21} & M_{22}\end{bmatrix}\begin{bmatrix}\rho\\ \theta\end{bmatrix}_1 \tag{1}$$

The matrix $[M]$ is constructed by multiplying the matrices $[M]_n \ldots [M]_2[M]_1$ for the elements of the optical system. There are only two kinds of elements needed: (a) translation through a distance d along the z-axis;

$$[M] = \begin{bmatrix}1 & d\\ 0 & 1\end{bmatrix} \tag{2}$$

(b) refraction at a curved interface of radius R (convex $R > 0$, concave $R < 0$) between two media with indices of refraction n_1 and n_2.

$$[M] = \begin{bmatrix}1 & 0\\ \dfrac{1}{R}\left(\dfrac{n_1}{n_2} - 1\right) & \dfrac{n_1}{n_2}\end{bmatrix} \tag{3}$$

5.1 Eye Model

The Gullstrand-Le Grand schematic model of the eye (Figure 9) is highly idealized, assumes all the surfaces are spherical and the eye is axisymmetric about the optical axis, which enables our simple ray tracing model to be applied. To obtain the $[M]$ matrix of the eye requires multiplying a total of 8 matrices, which represent the cornea (c), the aqueous humor (ah), the lens (l), and the vitreous humor (vh). The cornea and lens each require three matrices, one for the anterior surface (a), one for interior, and one for the posterior surface (p). The parameters of Table 2 (with one exception as discussed below) of these elements were taken from Gross et al. (2015); all dimensions are in mm. More sophisticated models are available (Atchison, 2006, Flores-Arias et al., 2009, Navarro, 2009) that could be used to refine the present results. The location of the retina relative to the lens posterior intersection with the optical axis was adjusted empirically to create the two accommodation models with a near point of 250 mm (4 Diopter) and 1000 mm (1 Diopter). These values were chosen to simulate the nominal near points (NP) of a 40 yr and $>$ 60 yr old (Gross et al., 2015).

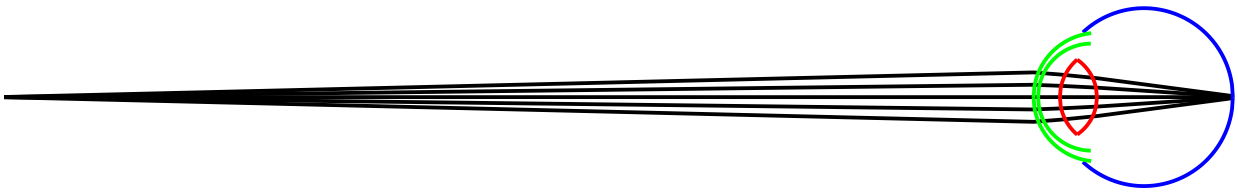

Figure 9: Schematic of Gullstrand-Le Grand eye model with representative rays imaging an object at the near point onto the retina.

Table 2: Geometric and refractive parameters used in the eye models.

	Relaxed			Accommodated				
				1000 mm NP			250 mm NP	
	n	R	z	n	R	z	R	z
gas	1			1				
cornea	1.3771	7.8	0	1.3771	7.8	0	7.8	0
		6.5	0.55		6.5	0.55	6.5	0.55
aqueous	1.3374			1.3374				
lens	1.42	10.2	3.6	1.427	6	3.2	6	3.2
		-6	7.6		-5.5	7.7	-5.5	7.7
vitreous	1.336			1.336				
retina		-10.5	24.2		-10.5	23.228	-10.5	23.16

Two additional matrices are required to model the gas layer, one for the vitreous humor-gas interface (with $R \to \infty$ for a flat interface) and one for the gas itself. For the purposes of the present modeling effort, the exact composition of the gas layer is not important and the results will apply equally to all gas mixtures (SF_6, C_3F_8 and mixtures with air) commonly used as tamponade. The index of refraction change across the gas-vitreous humor interface (-0.336) is much larger than variations in the index of refraction (less than 0.0008, see Table 3) due to gas mixture composition variation.

Table 3: Index of refraction for representative gases (Hayes, 2018) at 632.8 nm.

	n
air	1.00029
SF_6	1.000783
C_3F_8	1.00108

5.2 Conjugate focus location

An optical system like the schematic eye with fixed optical elements will only create a focused image of an object placed at the *conjugate focal location* to the retina. The determination of the conjugate focus is aided by recognizing that ray paths are reversible and a bundle of rays originating at the retina will be focused at the conjugate focal point. Consider a ray originating on the axis (ρ_1 = 0) at the conjugate focus location z_1 in front of eye and coming to focus on the retina at the axis ρ_2 = 0 with some unknown value of θ_2. Independent of the angle θ_1, the ray must return to ρ = 0. We can express this as the matrix equation

$$\begin{bmatrix} 0 \\ \theta_2 \end{bmatrix} = \begin{bmatrix} M_{11} & M_{12} \\ M_{21} & M_{22} \end{bmatrix} \begin{bmatrix} 1 & z_1 \\ 0 & 1 \end{bmatrix} \begin{bmatrix} 0 \\ \theta_1 \end{bmatrix} = \begin{bmatrix} M_{11} & M_{12} \\ M_{21} & M_{22} \end{bmatrix} \begin{bmatrix} z_1\theta_1 \\ \theta_1 \end{bmatrix} \tag{4}$$

and by inverting the matrix $[M]$, we can determine the z_1 from $z_1 = b_1/b_2$ independent of an arbitrarily chosen value of θ_2 where b_1 and b_2 are given by

$$\begin{bmatrix} b_1 \\ b_2 \end{bmatrix} = \begin{bmatrix} z_1\theta_1 \\ \theta_1 \end{bmatrix} = \begin{bmatrix} M_{11} & M_{12} \\ M_{21} & M_{22} \end{bmatrix}^{-1} \begin{bmatrix} 0 \\ \theta_2 \end{bmatrix} . \tag{5}$$

5.3 Magnification

Once the conjugate focus z_1 is determined, the lateral magnification m is defined as the ray height ρ_2 in the image plane of an object located at the conjugate focus and having a unit height $\rho = 1$.

$$\begin{bmatrix} m \\ \theta_2 \end{bmatrix} = \begin{bmatrix} M_{11} & M_{12} \\ M_{21} & M_{22} \end{bmatrix} \begin{bmatrix} 1 & z_1 \\ 0 & 1 \end{bmatrix} \begin{bmatrix} 1 \\ \theta_1 \end{bmatrix} \tag{6}$$

5.4 Tilted Interface

To model a tilted interface in conformation with Snell's law, an additional deflection needs to be added to the ray angle after applying the normal interface transformation matrix. The transformation of a ray moving from medium 1 to medium 2 through a slightly[8] tilted interface is given by

$$\begin{bmatrix} \rho_2 \\ \theta_2 \end{bmatrix} = \begin{bmatrix} 1 & 0 \\ 0 & n_1/n_2 \end{bmatrix} \begin{bmatrix} \rho_1 \\ \theta_1 \end{bmatrix} + \begin{bmatrix} 0 \\ 1 - n_1/n_2 \end{bmatrix} \psi \, . \tag{7}$$

where ψ is the angle measured from the perpendicular to the optical axis and positive for counterclockwise rotation.

5.5 Magnifying Lens

A thin lens consists of medium of index n_2 bounded by two surfaces close together with different radii of curvature, R_a and R_b and immersed in a medium with index n_1. If we ignore the thickness of the lens, the combined effect of the two interfaces is to act as a single lens element with a focal length f defined by

$$\frac{1}{f} = \left(\frac{n_1}{n_2} - 1 \right) \left(\frac{1}{R_a} - \frac{1}{R_b} \right) \, . \tag{8}$$

The ray transformation matrix is

$$\begin{bmatrix} 1 & 0 \\ -f^{-1} & 1 \end{bmatrix} \tag{9}$$

To determine the effect of using a magnifying lens in front of the eye, consider placing the lens at distance d_1 in front of the cornea and the object at a distance d_2 from the lens. The ray parameters at the retina will be obtained by using the following sequence of matrix operations on the ray parameters at the object.

$$\begin{bmatrix} \rho_2 \\ \theta_2 \end{bmatrix} = \underbrace{\begin{bmatrix} M_{11} & M_{12} \\ M_{21} & M_{22} \end{bmatrix} \begin{bmatrix} 1 & d_1 \\ 0 & 1 \end{bmatrix} \begin{bmatrix} 1 & 0 \\ -f^{-1} & 1 \end{bmatrix}}_{\text{magnifier-eye combination } M'} \begin{bmatrix} 1 & d_2 \\ 0 & 1 \end{bmatrix} \begin{bmatrix} \rho_1 \\ \theta_1 \end{bmatrix} = \begin{bmatrix} M'_{11} & M'_{12} \\ M'_{21} & M'_{22} \end{bmatrix} \begin{bmatrix} \rho_1 + d_2\theta_1 \\ \theta_1 \end{bmatrix} \tag{10}$$

If we require the distance d_2 to be the conjugate focus of the retina for the magnifier eye combination, then for points on the optical axis, $\rho_1 = \rho_2 = 0$ and the conjugate focus is determined by

$$\begin{bmatrix} 0 \\ \theta_2 \end{bmatrix} = \begin{bmatrix} M'_{11} & M'_{12} \\ M'_{21} & M'_{22} \end{bmatrix} \begin{bmatrix} d_2\theta_1 \\ \theta_1 \end{bmatrix} \, . \tag{11}$$

As with the case of the eye alone, the conjugate focus can be determined by using the inverse matrix to find $d_2 = b_1/b_2$.

$$\begin{bmatrix} b_1 \\ b_2 \end{bmatrix} = \begin{bmatrix} M'_{11} & M'_{12} \\ M'_{21} & M'_{22} \end{bmatrix}^{-1} \begin{bmatrix} 0 \\ \theta_2 \end{bmatrix} \tag{12}$$

[8]The angle cannot be too large or the paraxial ray approximation will not be valid.

6 Bubble shape

The bubble shape is determined by a delicate balance of the forces created by interfacial tension with the hydrostatic pressure difference due to gravity and the different in elevation of portions of the bubble surface. The balance between pressure difference ΔP across the gas-vitreous humor interface and surface tension is given by Young-Laplace equation (Batchelor, 1967, p. 65)

$$\Delta P = \gamma \left(\frac{1}{R_1} + \frac{1}{R_2} \right) \tag{13}$$

where γ = surface tension. The surface tension of the gas-vitreous humor interface is usually assumed (Eames et al., 2010, de Juan et al., 1985) to be similar to that of an air-water interface, which has $\gamma \approx 0.07$ N/m between 25 and 38°C. The pressure within the gas bubble is essentially constant, with a maximum possible variation of 10 Pa (0.07 mm Hg) between the top and bottom of the eye. The pressure difference across the gas-vitreous humor interface can be approximated by the hydrostatic pressure variation within the liquid alone which depends only on the elevation z of the interface at that location. Using the contact line location $z_c = S(r_c)$ on the retina as a reference, the pressure difference at other locations will be

$$\Delta P = P_{gas} - P_{vh} = \Delta P_c + \rho g (z - z_c) \quad \text{where} \quad \Delta P_c = \gamma \left(\frac{1}{R_1} + \frac{1}{R_2} \right)_{z_c} . \tag{14}$$

If we choose the location of the interface at the optical axis $z_\circ = S(0)$ as a reference then the pressure difference will be

$$\Delta P = P_{gas} - P_{vh} = \Delta P_\circ + \rho g (z - z_\circ) \quad \text{where} \quad \Delta P_\circ = \gamma \left(\frac{1}{R_1} + \frac{1}{R_2} \right)_{z_\circ} . \tag{15}$$

The forces are small but significant, the maximum hydrostatic pressure difference ($\rho g h$) possible within the eye is less than = 245 Pa (1.8 mm Hg). If the hydrostatic and surface tension forces are just in balance for a spherical bubble of radius a^* ($R_1 = R_2 = a^*$), this gives a typical size of a bubble which will have a strongly curved interface

$$a^* = \sqrt{\frac{\gamma}{2 g \rho}} . \tag{16}$$

Assuming a vitreous humor density ρ = 1000 kg/m^3, similar to water, the critical size a^* = 1.9 mm. Gas bubbles comparable to this radius or smaller will be spherical, bubbles that are much larger will be flattened on the anterior surface and the interface curvature will be concentrated near the intersection with the retina. The shape of the interface near the *contact line* or intersection of the gas-vitreous humor interface with the retina is determined by the balance of the interfacial forces including traction exerted on both gas and liquid by the retina.

This balance of forces results in the interface intersecting the surface of the retina at a well defined *contact angle* θ_c due to the traction on the vitreous humor by the retina pulling the contact line upward. For the contact between gas-vitreous humor and the retina, a range of values between 30 and 43° have been measured. Fawcett et al. (1994) made contact angle measurements using ex vivo retina specimens mounted on a flat surface (38.8±3.17°) and a flat protein-coated plastic surface (43.0±13.9°); Eames et al. (2010) used a spherical cavity with a protein-coated plastic surface (30.74±4.24°). In both sets of measurements, the gas was air and the vitreous humor was simulated by a water or phosphate-buffered saline solution. We have used a value of 39° in our simulations.

Away from the contact line, the Young-Laplace equation will determine how the elevation of the interface changes with radius, and influencing the curvature of the interface at the optical axis. Assuming a head-down position with a vertical optical axis, the bubble shape is symmetric about the optical axis and the analysis of the bubble shape is greatly simplified. Sufficiently close to the origin, the shape of the interface will be spherical and the principal radii of curvature are equal. The principal radii of curvature R_1 and R_2 are determined by the shape of the interface (O'Neill, 1966, p. 235), which can be computed from the interface shape function $S(r) = z$ and its derivatives

$$S' = \frac{\mathrm{d}S}{\mathrm{d}r} \quad \text{and} \quad S'' = \frac{\mathrm{d}^2 S}{\mathrm{d}r^2} . \tag{17}$$

The sum of the reciprocals of the principal radii of curvature (twice the mean curvature) for an axi-symmetric surface is

$$\frac{1}{R_1} + \frac{1}{R_2} = \frac{S''}{(1 + S'^2)^{3/2}} + \frac{1}{(1 + S'^2)^{1/2}} \frac{S'}{r} . \tag{18}$$

The specification of the interface location as a function $z = S(r)$ is logical but difficult to work with for a bubble since S is a multivalued function of r. Specifying $r = R(z)$ resolves that issue but some care is needed evaluating derivatives close to the axis ($r \to 0$ and $z \to z_\circ$). Using this alternative parameterization and defining

$$R' = \frac{\mathrm{d}R}{\mathrm{d}z} \quad \text{and} \quad R'' = \frac{\mathrm{d}^2R}{\mathrm{d}z^2} \,, \tag{19}$$

we can obtain an alternative expression for the sum of the reciprocals of the principal radii of curvature

$$\frac{1}{R_1} + \frac{1}{R_2} = -\frac{R''}{\left(R'^2+1\right)^{3/2}} + \frac{1}{\left(R'^2+1\right)^{1/2}}\frac{1}{R} \,. \tag{20}$$

The relationships between the derivatives of the quantities S and R are

$$\frac{\mathrm{d}S}{\mathrm{d}r} = \left(\frac{\mathrm{d}R}{\mathrm{d}z}\right)^{-1} \quad \text{and} \quad \frac{\mathrm{d}^2S}{\mathrm{d}r^2} = -\left(\frac{\mathrm{d}R}{\mathrm{d}z}\right)^{-3}\frac{\mathrm{d}^2R}{\mathrm{d}z^2} \,. \tag{21}$$

At the axis of symmetry, $r = 0$ and $z = z_\circ$, we have the following values for S and its derivatives

$$S(0) = z_\circ \,, \qquad S'(0) = 0 \,, \qquad S''(0) = \frac{1}{R_\circ} \geq 0 \,. \tag{22}$$

Using a Taylor series expansion of $S(r)$ near the axis, we can compute the quantities in the mean curvature expression through a limiting process

$$\lim_{r\to 0}\frac{S'(r)}{r} = S''(0) \,, \qquad \lim_{z\to z_\circ}\frac{1}{RR'(z)} = S''(0) \,, \qquad \lim_{z\to z_\circ}\frac{-R''(z)}{\left(R'(z)\right)^3} = S''(0) \,, \tag{23}$$

and

$$\left(\frac{1}{R_1} + \frac{1}{R_2}\right)_{r=0} = 2S''(0) \,. \tag{24}$$

At the contact line, $z = z_c$ and $r = r_c$, the interface must intersect the retina surface so that the included angle between the interface and retina is always θ_c. Referring to Figure 10, elementary trigonometry gives the relationship

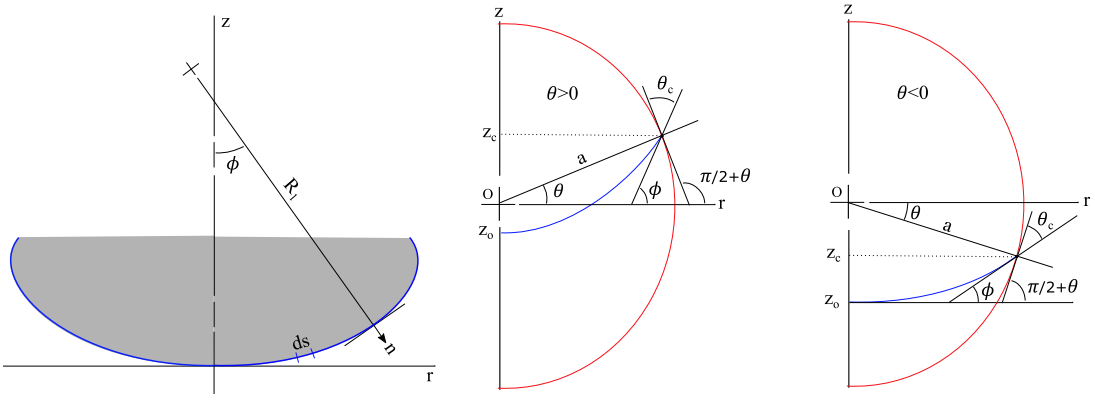

Figure 10: Geometry of a bubble interface showing the definition of the trigonometric parameters and variables used in the solution of the bubble shape.

between the angles to be

$$\phi - \theta = \frac{\pi}{2} - \theta_c \,, \tag{25}$$

where the angle ϕ of the interface relative to the horizontal reference is defined by

$$\tan\phi = \left(\frac{\mathrm{d}z}{\mathrm{d}r}\right)_{r_c} = S'(r_c) = \frac{1}{R'(z_c)} \; . \tag{26}$$

The angle θ of the contact line above the horizontal reference z = 0 is defined by the geometry as

$$\tan\theta = \frac{z_c}{\sqrt{a^2 - z_c^2)}} \; . \tag{27}$$

Using standard trigonometric identities we can write the contact angle condition as (taking care to select the appropriate branches of the tangent function).

$$R'(z_c) = \frac{1}{\tan\phi} = \frac{\tan\theta_c - \tan\theta}{1 + \tan\theta\tan\theta_c} \; . \tag{28}$$

The shape of the interface will be determined by integrating the differential equation resulting from applying the Young-Laplace equation on the interface. The domain of integration is between the axis of symmetry and the contact line, $z_\circ \le z \le z_c$ ($0 \le r \le r_c$). In terms of the parametrization $R(z)$, the equation is[9]

$$R'' + \left(R'^2 + 1\right)^{3/2}\left[\frac{2}{R_\circ} + \frac{\rho g}{\gamma}(z - z_\circ)\right] - \frac{\left(R'^2 + 1\right)}{R} = 0 \; . \tag{29}$$

One way to obtain a solution is to assume a location z_c of the contact line to find starting values

$$R(z_c) = \sqrt{a^2 - z_c^2} \; , \quad R'(z_c) = \frac{\tan\theta_c - \tan\theta}{1 + \tan\theta\tan\theta_c} \quad \text{where} \quad \tan\theta = \frac{z_c}{R(z_c)} \; . \tag{30}$$

Using these values and an assumed value of $R_\circ$ and $z_\circ$, the differential equation for R can be integrated from the contact line toward the axis of symmetry. As the interface approaches the optical axis, the interface flattens and the curvature decreases. Because the optical axis is an axis of symmetry for the surface and the surface is smooth and without kinks, the interface slope has to smoothly approach zero, i.e., $R' \to \infty$ as $z \to z_\circ$. Upon reaching R = 0 (the axis), the value of $z = z_b$ and the radius of curvature can be computed and checked for consistency with the assumed values. Unfortunately, this is difficult to do in practice because of the singularity of R' at the origin and need to simultaneously solve for $R_\circ$ and $z_\circ$.

6.1 Adams' Formulation

Computing the surface shape with either the $S(r)$ or $R(z)$ shape function is difficult to implement numerically as a two-point boundary value problem. Both the height z_c of the interface and the radius of curvature $R_\circ$ at the origin are unknown and have to be sought as part of the solution, which is very sensitive to these values, making it difficult to obtain convergence. Solutions that employ $R(z)$ and integrate in z from z_c to $z_\circ$ are singular at the origin where $R'(0)$ = ∞. Solutions that employ $S(r)$ to integrate in r from r = 0 to r_c can potentially have an internal singularity S' =∞ when the interface is vertical and the direction of integration in r changes sign at this point.

J.C. Adams[10] discovered an alternative formulation (Bashforth and Adams, 1883, Ch. III) that solves all these problems and is straightforward to integrate numerically. Adams uses the angle of the surface normal ϕ or arc length s and the meridional radius of curvature R_1 as the independent variables. Adams also simplified the notation by scaling all lengths in terms of the radius of curvature $R_\circ$ at the origin and introduced a single nondimensional parameter to characterize the relative effects of surface tension and gravity. The scaled variables are

$$\tilde{r} = \frac{r}{R_\circ} \quad \tilde{z} = \frac{z}{R_\circ} \quad \varrho = \frac{R_1}{R_\circ} \; , \tag{31}$$

[9] Eames et al. (2010) take this approach but the equations given in their appendix are incorrect, there is a sign error in the boundary condition and the Young-Laplace equation is missing the term $2/R_\circ$.

[10] British mathematician and astronomer (b. 1818-d. 1892) who predicted the existence of the planet Neptune. Goldstine (1977) discusses the historical context of Adams' work and states (Goldstine, 1977, p. 205) that the method of solution presented in Ch. III of Bashforth and Adams (1883) should be credited to Adams alone.

and the equations are

$$\frac{\mathrm{d}\tilde{r}}{\mathrm{d}\phi} = \varrho \cos\phi \,, \tag{32}$$

$$\frac{\mathrm{d}\tilde{z}}{\mathrm{d}\phi} = \varrho \sin\phi \,, \tag{33}$$

where the scaled meridonal radius of curvature $\varrho = R_1/R_\circ$ is defined by the Young-Laplace equation in the form

$$\frac{1}{\varrho} + \frac{\sin\phi}{\tilde{r}} = 2 + \beta\tilde{z} \,, \tag{34}$$

and $\beta = R_\circ^2 \rho g/\gamma$ is the *Bond number*. The relationship of the variables ϱ and ϕ to the derivatives of $z(r)$ are

$$\frac{1}{\varrho} = \frac{\dfrac{\mathrm{d}^2\tilde{z}}{\tilde{r}}}{\left[1 + \left(\dfrac{\mathrm{d}\tilde{z}}{\mathrm{d}\tilde{r}}\right)^2\right]^{3/2}} \tag{35}$$

$$\sin\phi = \frac{\dfrac{\mathrm{d}\tilde{z}}{\mathrm{d}\tilde{r}}}{\left[1 + \left(\dfrac{\mathrm{d}\tilde{z}}{\mathrm{d}\tilde{r}}\right)^2\right]^{1/2}} \tag{36}$$

The equations for $\tilde{r}$ and $\tilde{z}$ can be integrated from the origin for assumed value of β (or equivalently $R_\circ$) using the initial conditions

$$\tilde{r} = 0 \quad \text{at} \quad \phi = 0 \,, \tag{37}$$

$$\tilde{z} = 0 \quad \text{at} \quad \phi = 0 \,. \tag{38}$$

The choice of $\tilde{z} = 0$ at the origin is arbitrary and for the situation of a bubble within an eye, will be determined after the contact angle condition is applied at the bubble boundary. Near the origin, Adams determined the following power series expansions in ϕ.

$$\tilde{r} = \phi - \left(\frac{1}{6} + \frac{1}{8}\beta\right)\phi^3 + \left(\frac{1}{120} + \frac{1}{24}\beta + \frac{1}{24}\beta^2\right)\phi^5 - \dots \,, \tag{39}$$

$$\tilde{z} = \frac{1}{2}\phi^2 - \left(\frac{1}{24} + \frac{3}{32}\beta\right)\phi^4 + \left(\frac{1}{720} + \frac{1}{72}\beta + \frac{5}{144}\beta^2\right)\phi^6 - \dots \,, \tag{40}$$

$$\frac{1}{\varrho} = 1 + \frac{3}{8}\beta\phi^2 + \left(-\frac{1}{48}\beta - \frac{13}{192}\beta^2\right)\phi^4 + \left(\frac{111}{5760}\beta + \frac{1}{128}\beta^2 + \frac{229}{9216}\beta^3\right)\phi^6 \dots \,. \tag{41}$$

These results can be used to show that at the origin

$$\lim_{\phi\to 0} \frac{\sin\phi}{\tilde{r}} = 1 \,. \tag{42}$$

Adams actually computed these expansions up to the 11th power in ϕ but I have only used the first three terms to initialize my solution. Adams points out that using ϕ as an independent variable is appropriate only as long as $\beta > 0$ (gas bubbles) and shows that using arc length s is a more general solution that also works for $\beta < 0$, the case of liquid drops. The revised set of differential equations in terms of scaled arc length $\tilde{s} = s/R_\circ$:

$$\frac{\mathrm{d}\phi}{\mathrm{d}\tilde{s}} = \frac{1}{\varrho} \,, \tag{43}$$

$$\frac{\mathrm{d}\tilde{r}}{\mathrm{d}\tilde{s}} = \cos\phi \,, \tag{44}$$

$$\frac{\mathrm{d}\tilde{z}}{\mathrm{d}\tilde{s}} = \sin\phi \,. \tag{45}$$

and Adams gives the expansions near the origin in terms of $\tilde{s}$ as

$$\phi = \tilde{s} + \frac{1}{8}\beta\tilde{s}^3 + \left(-\frac{1}{240}\beta^+\frac{1}{192}\beta^2\right)\tilde{s}^5 + \left(\frac{11}{40320}\beta - \frac{11}{13440}\beta^2 + \frac{1}{9216}\beta^3\right)\tilde{s}^7 - \dots\,, \tag{46}$$

$$\tilde{r} = \tilde{s} - \frac{1}{6}\tilde{s}^3 + \left(\frac{1}{120} - \frac{1}{40}\beta\right)\tilde{s}^5 - \left(\frac{1}{5040} - \frac{1}{280}\beta + \frac{5}{2688}\beta^2\right)\tilde{s}^7 - \dots\,, \tag{47}$$

$$\tilde{z} = \frac{1}{2}\tilde{s}^2 + \left(-\frac{1}{24} + \frac{1}{32}\beta\right)\tilde{s}^4 + \left(\frac{1}{720} - \frac{1}{90}\beta + \frac{1}{1152}\beta^2\right)\tilde{s}^6 - \dots\,, \tag{48}$$

$$\frac{1}{\varrho} = 1 + \frac{3}{8}\beta\tilde{s}^2 + \left(-\frac{1}{48}\beta + \frac{5}{192}\beta^2\right)\tilde{s}^4 + \left(\frac{11}{5760}\beta - \frac{11}{1920}\beta^2 + \frac{7}{9216}\beta^3\right)\tilde{s}^6 \dots\,. \tag{49}$$

Adams developed what is known today as the Adams-Bashforth predictor-corrector method (Bashforth and Adams, 1883, See Ch. III) for solving the differential equation system using the series expansion to obtain the starting values. This method was used to create the tables in Bashforth and Adams of numerical values of the normalized interface shape for Bond numbers between 0.125 and 100. My numerical solutions were carried out with MATLAB 2018a and the stiff integration method `ode15s` with relative and absolute tolerances of 10^{-12}; the first three terms of Adams' small angle expansion were used to start the solution at ϕ = 10^{-7}. Comparison of the 1883 tabulation and 2018 solutions (Figure 11) verifies that the differences between the $(\tilde{r}, \tilde{z})$ values for two solutions at a given value of ϕ are at most ± 1 in the least significant digit over the entire surface.[11]

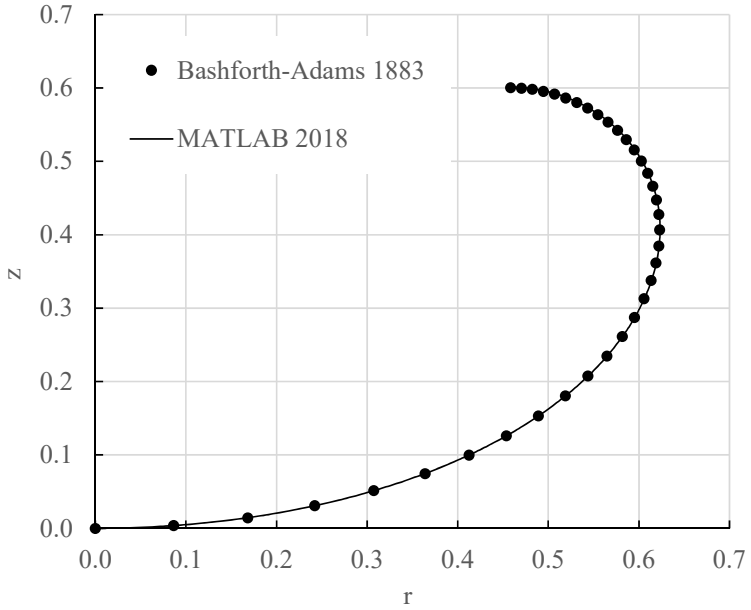

Figure 11: Comparison of the Bashforth and Adams (1883) tabulated solution for β = 9 with current MATLAB integration results.

6.2 Volume and Coverage Angle

The volume of a gas bubble can be computed by integration using the radius as a function of vertical distance, $r(z)$.

$$V = \int_{z_\circ}^{a} \pi r^2(z)\,\mathrm{d}z \tag{50}$$

[11]The tables in Bashforth and Adams give the results to five significant digits for values of ϕ from 0 to 180° in 5° increments.

The integration has to be carried out numerically for the portion of the bubble below the contract line (z = z_c) but an analytical expression can be obtained for the spherical cap above the contact line

$$V = V_{bub} + V_{cap} \ , \tag{51}$$

where the bubble volume below the contact line is

$$V_{bub} = \int_{z_\circ}^{z_c} \pi r^2(z) \mathrm{d}z \ . \tag{52}$$

The volume of the cap is most simply computed using the angle θ as the independent variable. For a sphere of radius a, the volume of the cap is

$$V_{cap}(\theta) = \pi a^2 \left(\frac{2}{3} - \sin\theta + \frac{1}{3}\sin^3\theta \right) \ . \tag{53}$$

The coverage angle is the angle subtended by the portion of the retina covered by gas in the head down position.

$$\theta_{cov} = \pi - 2\theta \tag{54}$$